Molecular Biology of the Cell
Vol. 20, 5074–5085, December 15, 2009

Myosin IXa Regulates Epithelial Differentiation and Its Deficiency Results in Hydrocephalus

Marouan Abouhamed,*† Kay Grobe,*†‡ Isabelle V. Leefa Chong San,§ Sabine Thelen,* Ulrike Honnert,* Maria S. Balda,§ Karl Matter,§ and Martin Bähler*

*Institute of General Zoology and Genetics, Westfalian Wilhelms University, 48149 Münster, Germany; and §Department of Cell Biology, UCL Institute of Ophthalmology, University College London, London EC1V 9EL, United Kingdom

Submitted April 10, 2009; Revised October 5, 2009; Accepted October 7, 2009
Monitoring Editor: Josephine C. Adams

The ependymal multiciliated epithelium in the brain restricts the cerebrospinal fluid to the cerebral ventricles and regulates its flow. We report here that mice deficient for myosin IXa (Myo9a), an actin-dependent motor molecule with a Rho GTPase–activating (GAP) domain, develop severe hydrocephalus with stenosis and closure of the ventral caudal 3rd ventricle and the aqueduct. Myo9a is expressed in maturing ependymal epithelial cells, and its absence leads to impaired maturation of ependymal cells. The Myo9a deficiency further resulted in a distorted ependyma due to irregular epithelial cell morphology and altered organization of intercellular junctions. Ependymal cells occasionally delaminated, forming multilayered structures that bridged the CSF-filled ventricular space. Hydrocephalus formation could be significantly attenuated by the inhibition of the Rho-effector Rho-kinase (ROCK). Administration of ROCK-inhibitor restored maturation of ependymal cells, but not the morphological distortions of the ependyma. Similarly, down-regulation of Myo9a by siRNA in Caco-2 adenocarcinoma cells increased Rho-signaling and induced alterations in differentiation, cell morphology, junction assembly, junctional signaling, and gene expression. Our results demonstrate that Myo9a is a critical regulator of Rho-dependent and -independent signaling mechanisms that guide epithelial differentiation. Moreover, Rho-kinases may represent a new target for therapeutic intervention in some forms of hydrocephalus.

INTRODUCTION

The development and homeostasis of multicellular organisms depends on coordinated cell shape changes that are coupled with alterations in intracellular organization. The dynamic organization of the actin cytoskeleton accounts for many cell shape changes. A multitude of proteins can directly or indirectly modify the dynamics and organization of the actin cytoskeleton. Among these proteins are monomeric GTPases and the superfamily of myosin molecules. The myosin superfamily of actin-based molecular motors is subdivided into more than 30 classes (Odronitz and Kollmar, 2007). The class IX of myosin molecules includes in mammals two members, Myo9a (myr 7) and Myo9b (myr 5), that are both expressed in a number of differentially spliced variants (Bähler, 2008). The Myo9a protein, previously also called myr 7, is expressed during development and in many adult tissues, most abundantly in brain and testis (Chieregatti *et al.*, 1998; Gorman *et al.*, 1999). Class IX myosins comprise in addition to their myosin head domain a tail region that encompasses a C1 domain and a Rho GTPase-activating protein (RhoGAP) domain (Reinhard *et al.*, 1995; Chieregatti *et al.*, 1998). The RhoGAP domain negatively regulates the monomeric Rho GTPase by accelerating its rate of GTP-hydrolysis, switching it from the active GTP-bound form to the inactive GDP-bound form. The RhoGTPases are known to be important regulators of cell morphogenesis, cell migration, and cell proliferation (Jaffe and Hall, 2005). They are inactivated under spatial and temporal control by roughly 70 mammalian RhoGAP family members (Bernards, 2003). To understand the in vivo importance of limiting Rho activity by RhoGAPs, it is necessary to delete individual RhoGAPs.

The RhoGAP domain of Myo9a inactivates in vitro Rho A, B, C and the overexpression of Myo9a in cells causes morphological alterations characteristic for Rho A inactivation (Chieregatti *et al.*, 1998). However, nothing is currently known about the physiological function of the Myo9a-RhoGAP.

A major tissue type of vertebrates constitutes the epithelium. The formation of epithelia depends on the development of specific cell–cell adhesion structures between neighboring cells and the establishment of cell polarity. An intricate spatial regulation of Rho activity and its downstream effectors Rho-kinase (ROCK) and diaphanous (Dia) was implicated in the stabilization and maintenance of tight junctions and adherens junctions (Sahai and Marshall, 2002; Aijaz *et al.*, 2005; Ozdamar *et al.*, 2005; Samarin *et al.*, 2007;

This article was published online ahead of print in *MBC in Press* (http://www.molbiolcell.org/cgi/doi/10.1091/mbc.E09–04–0291) on October 14, 2009.

† These authors contributed equally to this work.

‡ Present address: Physiological Chemistry and Pathobiochemistry, University of Münster, Münster D-48149, Germany.

Address correspondence to: Martin Bähler (baehler@uni-muenster.de).

Abbreviations used: CSF, cerebrospinal fluid; Myo9a, myosin IXa; RhoGAP, Rho GTPase-activating protein; ROCK, Rho-kinase; WT, wild type.

Yamada and Nelson, 2007; Fang *et al.*, 2008; Homem and Peifer, 2008). These junctional complexes are not only important for the barrier function of epithelia, but they also regulate cell proliferation and differentiation (Balda and Matter, 2003).

The ventricular system in the vertebrate brain is lined by a single-layered, isoprismatic to columnar, multiciliated epithelium, called the ependyma. The cilia on the lumenal surface propel the cerebrospinal fluid (CSF) through the ventricular system from the two symmetrical lateral ventricles to the third ventricle and on through the aqueduct to the fourth ventricle. From there the CSF enters the spinal canal and subarachnoid space where it gets resorbed. It has been shown that mutations in ciliary components that affect the proper generation or beating of cilia cause an enlargement of ventricles and hydrocephalus (Sapiro *et al.*, 2002; Ibañez-Tallon *et al.*, 2004; Banizs *et al.*, 2005; Lechtreck *et al.*, 2008). Similarly, the loss of a number of proteins thought to affect adhesion and polarity such as Dlg5, Numb/Numbl, myosin IIB, PKCλ, and oligophrenin was implicated in inducing hydrocephalus by affecting the integrity of the ependyma (Imai *et al.*, 2006; Kuo *et al.*, 2006; Khelfaoui *et al.*, 2007; Ma *et al.*, 2007; Nechiporuk *et al.*, 2007).

In this study we thought to determine the function of the RhoGAP Myo9a in mammalian development and homeostasis. To this end, we generated mice deficient for Myo9a protein and down-regulated Myo9a in Caco-2 cells. The mice developed a severe hydrocephalus with enlarged lateral and third ventricles and stenosis of the ventral part of the third ventricle and the aqueduct. The ependymal epithelial cells in the ventral 3rd ventricle and in the aqueduct revealed alterations in cell morphology, tight and adherens junctions, and cell differentiation. Similar effects were noted in Caco-2 cells after down-regulation of Myo9a expression. Reducing the activity of Rho-kinase, a downstream effector of Rho, but not of RhoB, attenuated the development of hydrocephalus.

MATERIALS AND METHODS

Targeted disruption of Myo9a

The generation of Myo9a deficient mice is described in Supplemental Material.

In Situ Hybridization

In situ hybridizations were essentially performed according to the protocol described on http://wmc.rodentia.com/docs/Big_In_Situ.html. Brains of mice at embryonic day 17.5 and postnatal day 0.5 (P0.5) and P3.5 were flash-frozen in liquid nitrogen and embedded in tissue-freezing medium (Jung, Leica Microsystems, Nussloch, Germany). Frozen sections of 10 μm thickness were prepared in a refrigerated microtome (Leica CM 1900) and mounted on Superfrost plus glass slides (Thermo Scientific, Braunschweig, Germany). Slides were dried at 50°C, and tissue sections were fixed with 4% PFA in phosphate-buffered saline (PBS). Tissue was permeabilized with 1 μg/ml proteinase K (AppliChem, Darmstadt, Germany) for 5 min at room temperature (RT). Specimens were then fixed again in 4% PFA. To block unspecific binding, tissue was treated with 0.25% (vol/vol) acetic anhydride in triethanolamine buffer. Sections were prehybridized in hybridization buffer (50% [vol/vol] formamide, 5× SSC, 1 mg/ml yeast tRNA, 100 μg/ml heparin, 1× Denhardt's solution, 0.1% Tween 20, 0.1% CHAPS, and 5 mM EDTA) for 4 h, drained, and hybridized overnight at 60°C in a humid chamber with 1.5 μg/ml labeled sense or antisense probe in hybridization buffer. The slides were covered with parafilm to reduce evaporation. After hybridization, slides were washed once with 1× SSC and 1.5× SSC at 60°C and twice in 2× SSC at 37°C. After washing stringently, tissue was treated with 0.2 μg/ml RNAse A (Diagonal, Münster, Germany) in 2× SSC for 30 min at 37°C. Thereafter, the sections were washed in the following solutions: 2× SSC (10 min at RT), 0.2× SSC (twice for 30 min each at 60°C), and PTw (1× PBS, 0.1% Tween 20; twice for 10 min at 60°C and 10 min at RT), followed by PBT (1× PBS, 2 mg/ml BSA, 0.1% Triton X-100) for 15 min at RT. Unspecific antibody binding sites were blocked by incubation with 20% heat-inactivated sheep serum (PAA Laboratories, Pasching, Austria) in PBT for 3 h at RT. Subsequently, specimens were incubated with sheep anti-digoxigenin Fab-fragments (Roche Diagnostics, Mannheim, Germany) conjugated with alkaline phosphatase (1:2000 in 20% sheep serum in PBT) overnight at 4°C. After washing with PBT and inhibition of endogenous alkaline phosphatase activity with 5 mM tetramisole (Sigma-Aldrich, Steinheim, Germany), bound alkaline phosphatase was visualized by incubation with 6 μl/ml NBT (nitroblue tetrazolium)/BCIP (5-bromo-4-chloro-3-indolyl phosphate) substrate in alkaline buffer for several hours. Tissue then was fixed and mounted for analysis under a stereomicroscope (Leica MZ 125) equipped with a camera (Leica DFC 280).

As a probe, a 3′-UTR Myo9a fragment of 744 base pairs (Allen Brain Atlas, specimen ID 05-0849; http://www.brain-map.org/) was amplified by PCR using primers 5′-TGATCTGATAGAGACGAAGCCA-3′ and 5′-TAACTCT-CAGCGTCACACACCT-3′ and cloned into pGEM-T easy (Promega, Madison, WI). Antisense and sense cRNA probes were transcribed in vitro using the linearized plasmid (NcoI or SalI) and the DIG RNA labeling kit (Roche Diagnostics, Mannheim, Germany) according to manufacturer's instructions. Concentrations of probes were determined with dot-blot analysis and the DIG nucleic acid detection kit (Roche Diagnostics).

Histochemistry and Immunohistochemistry

Embryos and brains from newborn or young mice were fixed in Bouin's fixative (Sigma-Aldrich) for 18–30 h and then cleared and conserved in 70% (vol/vol) ethanol. They were then dehydrated, embedded in paraffin, sectioned at 8–15 μm, and stained with hematoxylin and eosin (H&E) for histological analysis or with antibodies for immunofluorescence and immunohistochemistry.

For staining with the antibodies against S100, β-catenin, E-cadherin, acetylated α-tubulin, Myo9a, proliferating cell nuclear antigen (PCNA), and JamA, sodium citrate (0.3% sodium citrate 0.05% Tween 20, pH 6.0) heat antigen retrieval was performed. For the staining of occludin, protease type XIV from *Streptomyces griseus* (1 μg/μl; Sigma-Aldrich) enzymatic antigen retrieval was required for 20 min at 37°C. Sections were subsequently permeabilized with 1% Triton X-100 (15 min, RT) and blocked by incubation in blocking buffer (5% normal goat serum, 1% BSA, 0.05% Tween-20, 0.1% Triton X-100, and 0.75% glycine in PBS) for 1 h at RT. Sections were incubated at 4°C over night with primary antibodies against β-catenin and occludin (all 1:400; Zymed, South San Francisco, CA), S100 (1:500; Dako, Glostrup, Denmark), E-cadherin (1:400; Upstate Biotechnology, Lake Placid, NY), PCNA (1:1000; Abcam, Cambridge, MA), Myo9a (1:1000, Tü78 affinity-purified; Chieregatti *et al.*, 1998), acetylated α-tubulin (1:50; Woods *et al.*, 1989), and Jam A (1:100; a generous gift from K. Ebnet, Zentrum für Molekularbiologie der Entzündung, Münster, Germany). After washing, Myo9a was visualized using horseradish peroxidase–conjugated secondary antibodies (1:500; Jackson ImmunoResearch Laboratories, West Grove, PA) and 3,3′diamino-benzidine-tetrahydrochloride (DAB) substrate (Sigma-Aldrich). For indirect immunofluorescence labeling, we used either Cy3-conjugated secondary antibodies (all 1:250; Jackson ImmunoResearch Laboratories) and/or Alexa488-conjugated secondary antibodies (1:300; Molecular Probes, Eugene, OR). Nuclei were stained with DAPI (4 μg/ml; Sigma-Aldrich). Finally, all sections were rinsed in PBS and mounted in Mowiol. Stainings were visualized using either an Axiophot fluorescence microscope (Carl Zeiss, Jena, Germany) equipped with an ORCA-285 digital camera (Hamamatsu Photonics, Herrsching, Germany) controlled by Wasabi software (version 1.4; Hamamatsu) or the LSM 510 confocal microscope (Carl Zeiss) with LSM Release 4.2 software.

Oral Administration of ROCK-Inhibitor Y-27632

The protocol was adapted from that described by Nagatoya *et al.* (2002). Timed pregnant mice were obtained by overnight breeding Myo9a$^{+/-}$ mice and checking for vaginal plugs the next morning. The presence of a vaginal plug was defined as gestational day E0.5 (embryonic day 0.5). Pregnant mice (E12.5) were divided into two groups: a vehicle control group (n = 14) that was maintained on tap water with 30% sucrose (wt/vol) and standard chow and a Y-27632 group (n = 10) that was maintained on tap water with ROCK-inhibitor Y-27632, (200 mg/l; Tocris Cookson, Bristol, United Kingdom), 30% sucrose (wt/vol), and standard chow. The two groups were treated from E12.5 until P3.5. Then paraffin sections were prepared from the brains of the pups. They were stained with H&E for morphometric analysis. The areas of the lateral ventricle at the position of the anterior commissure and the areas of the total brain section were measured using MetaMorph software (version 3.5; Universal Imaging, West Chester, PA).

Maintenance of Caco-2 Cells and Depletion of Myo9a by RNAi

Caco-2 cells were cultured as described and plated in 48- or 96-well plates for experiments (Matter *et al.*, 1989). Control and Myo9a siRNAs were obtained from Dharmacon (Lafayette, CO)/Thermo Fisher Scientific, using siGenome smart pools for a first set of experiments and ON-TARGETplus smart pools for all experiments shown in this article. Both sets of siRNAs gave similar results. Cells were transfected with DharmaFECT-4 according to the manufacturer's instructions. Protein expression was analyzed after 72 h (Balda *et al.*, 1996).

Analysis of Caco-2 Cells by Immunofluorescence and Reporter assays

For immunofluorescence, the cells were cultured on glass coverslips in 48-well plates. Seventy-two hours after the siRNA transfection, the cells were

fixed in methanol and labeled by indirect immunofluorescence (Balda *et al.*, 2003). Antibodies against DPPIV, NaK-ATPase, α-tubulin, ZO-1, and ZONAB were previously described (Balda *et al.*, 2003; Benais-Pont *et al.*, 2003; Hauri *et al.*, 1985; Kreis, 1987). Goat anti-β-catenin was obtained from Santa Cruz Biotechnology (Santa Cruz, CA); mouse anti-ZO-2, mouse anti-occludin, and rabbit anti-claudin-1 were from Invitrogen (Carlsbad, CA); and mouse anti-E-cadherin was from BD Biosciences (Heidelberg, Germany). All secondary antibodies were from Jackson ImmunoResearch Laboratories. Images were obtained with a Leica DM1 RB microscope equipped with a 63×/1.4 NA oil immersion objective and a Hamamatsu ORCA285 camera or a Leica SP2 confocal microscope also with a 63×/1.4 NA oil immersion objective. Image brightness and contrast were adjusted with Adobe Photoshop (San Jose, CA). For reporter assays, the cells were plated in 96-well plates. Twenty-four hours after the small interfering RNA (siRNA) transfection, firefly luciferase reporter plasmids for β-catenin/T-cell factor (TCF), ZONAB, nuclear factor κB (NF-κB), and serum response element (SRE) were transfected along with a control promoter lacking such regulatory elements driving renilla luciferase expression (van de Wetering *et al.*, 1997; Balda and Matter, 2000; Aijaz *et al.*, 2005; Frankel *et al.*, 2005). After another 48 h, the cells were lysed and expression of the two luciferases was assayed (Tsapara *et al.*, 2006). Expression of renilla luciferase was used as a transfection control.

Statistical Analysis

Representative data or means ± SEM are shown. Statistical analysis using unpaired Student's *t* test was carried out with OriginPro 07. For more than two groups one-way ANOVA with Tukey post hoc test was used. Results with $p \leq 0.05$ were considered to be statistically significant.

RESULTS

Generation of Myo9a Knockout Mice

To characterize the functional role of the RhoGAP Myo9a in vertebrates, we generated mice deficient in Myo9a protein (Supplementary Figure S1). Exon 2 of Myo9a, including part of the 5′UTR and coding for the N-terminal 280 of 2542 amino acids of the protein, was flanked by Cre/LoxP recombination sequences and a neomycin selection cassette flanked by FRT recombination sites in embryonic stem cells by homologous recombination. Breeding of resulting transgenic mice with FLPe transgenic mice (Rodríguez *et al.*, 2000) resulted in the removal of the neomycin cassette and breeding with ZP3-Cre mice (De Vries *et al.*, 2000) in the generation of Myo9a systemic (type I) mutant mice. Deletion of exon 2 resulted in completely abolished Myo9a protein expression as confirmed by Western blot analysis of protein extracts derived from homozygous mutant mice using polyclonal anti-Myo9a antisera (Supplementary Figure S1D). We thus concluded that we have generated mice with the null allele of Myo9a.

Myo9a-deficient Mice Develop Severe Postnatal Hydrocephalus and Stenosis of the Ventral Caudal 3rd Ventricle and the Aqueduct

In contrast to wild-type (WT) and heterozygous mice, Myo9a-deficient mice displayed a retarded growth and developed a dome-shaped skull characteristic for hydrocephalus within the first 2 wk of life (Figures 1, A and B). Surviving adult mice also showed a hopping/trembling gait similar to hydrocephalic (hyh) and Dlg5$^{-/-}$ mice (Chae *et al.*, 2004; Nechiporuk *et al.*, 2007). Gross examination and histological analysis of Myo9a-deficient brains indeed revealed fully penetrant hydrocephalus (n = 53) with massive dilation of the lateral ventricles and the 3rd ventricle, but never of the 4th ventricle (Figure 1, C–H). Such alterations were never observed in WT or heterozygous mice.

To determine the cellular defect resulting in the formation of hydrocephalus, we analyzed serial sections of P0.5, P3.5, and P14.5 WT and Myo9a$^{-/-}$ brains histologically. In brains of WT mice the ventral caudal 3rd ventricle formed a continuous elongated duct that was lined by a smooth ependyma (Figure 1, H and I). On the contrary, in all Myo9a-deficient brains investigated (n = 16) the ventral caudal 3rd ventricle was distorted and closed (Figure 1, G and I). Ependymal cells lining the ventral caudal 3rd ventricle were disorganized and absent in areas of ventricle closure. Between P0.5 and P14.5 the aqueduct connecting the 3d and 4th ventricle also became progressively narrower and ultimately closed in mutant mice (Figure 1J). The symmetrically bilobed canal at the dorsal side of the rostral aqueduct was generally asymmetric and distorted in the mutant mice (Figure 1J). Similarly to the situation in the ventral caudal 3rd ventricle, the aqueduct was partially closed forming two separate small lumens lined by ependymal epithelial cells instead of a single elongated continuous connection. In the median aqueduct, especially in vaults, discontinuities with denudations of the ependymal epithelial layer were noted (Figure 1, J–L). Irregularities in the ependymal lining were frequently seen in the two affected regions of the ventricular system. We conclude that CSF flow is impaired by progressive closure of the ventral caudal 3rd ventricle and the aqueduct. Notably, lateral ventricles and the 3rd ventricle rostral to the closed region were highly dilated, whereas the 4th ventricle and subarachnoid space were normal in all mutant mice. Therefore, the stenosis and closure of the ventricular system already observed in newborn mice are the likely cause for the concomitant accumulation of CSF in the lateral ventricles and part of the 3rd ventricle.

Myo9a Is Expressed in the Ependymal Cell Layer of the Ventral Caudal 3rd Ventricle and Aqueduct

In situ hybridization was performed to elucidate the expression of Myo9a during embryonic and postnatal development of the mouse brain. At E17.5, Myo9a expression was not detectable in the ventral median 3rd ventricle, but it was expressed in a spotty pattern in the developing aqueduct (Figure 2A, top). At P0.5, Myo9a expression was clearly detectable in ependymal cells lining the ventral 3rd ventricle and the aqueduct, as well as in surrounding tissue (Figure 2A, middle). Myo9a continued to be expressed in ependymal cells of both the 3rd ventricle and the aqueduct at P3.5. We also investigated Myo9a expression immunohistochemically in P3.5 brain tissue sections using an affinity-purified Myo9a antibody. Prominent Myo9a staining was observed in ependymal cells lining the ventral 3rd ventricle and aqueduct in WT mice (Figure 2, B and C), but not in Myo9a$^{-/-}$ mutants, confirming Myo9a expression in ependymal cells. Myo9a was observed in the cytosol and was enriched at the junctional complexes (Figure 2, B and C). These results demonstrate that Myo9a is expressed in the ependymal cells at the developmental time during which alterations were observed in mice deficient for Myo9a.

Myo9a Deficiency Perturbs Cell Shape and Cell Contacts in the Ependymal Epithelium of the Ventral Caudal 3rd Ventricle and the Aqueduct

A close inspection of the ventricular surface of the ventral caudal 3rd ventricle and the aqueduct using junctional markers (E-cadherin, β-catenin) revealed that it was considerably undulated in Myo9a$^{-/-}$, but linear in brains from WT mice (Figure 3, A–D). Sections along the plane of the ependymal epithelium confirmed that the undulated appearance was due to changes in cell shape (Figure 3, E and F). The overall outline of the cells marked by adherens junctions was distorted. The cell–cell boundaries were bent and strained compared with those in WT ependyma, suggesting that these junctions experienced unequal tension. We quantified this difference by measuring the ratio of junction length to the distance between vertices, defining a "lin-

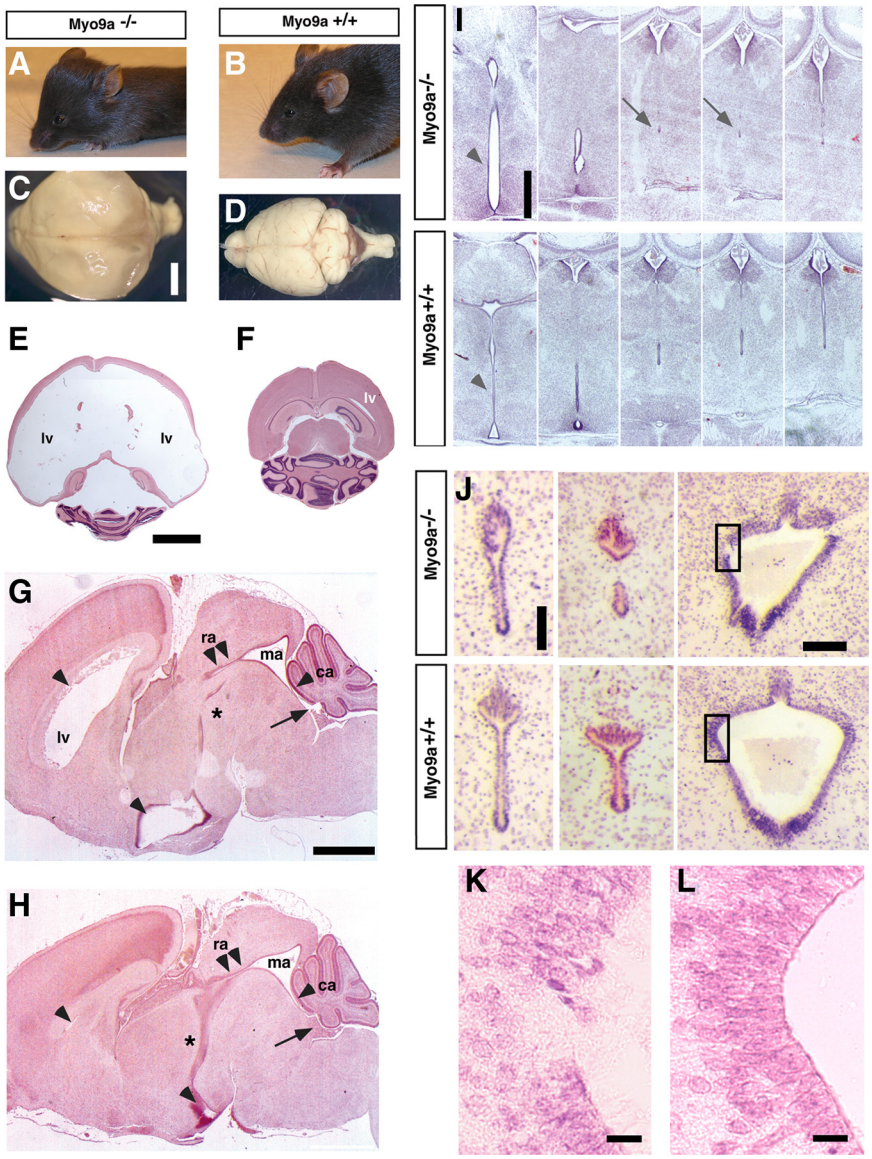

Figure 1. Myo9a-deficient mice develop hydrocephalus and stenosis of the ventral caudal 3rd ventricle and the aqueduct. (A and B) Comparison of lateral views of 21.5-d-old Myo9a$^{-/-}$ and WT mice. All mutant mice (>P7.5, n = 23) display a domed skull characteristic of hydrocephalus. (C and D) Global brain analysis shows enlarged hemispheres and compressed olfactory bulbs/cerebellum in the mutant mice (C) compared with WT (D). Hydrocephalus was never detected in any of the WT or heterozygous mice (n = 63) as well as homozygous type II (floxed) control animals (n = 98), demonstrating that the transgene did not result in hydrocephalus formation per se. (E and F) H&E-stained horizontal sections through identical areas of the brain demonstrate extreme dilation of the lateral ventricles in P14.5 mutant animals (E) compared with the WT littermate controls (F). (G and H) H&E-stained sagittal brain sections demonstrate dilation of the lateral ventricles (lv) and the ventral 3rd ventricle (arrowheads), but not of the fourth ventricle (arrow), in P3.5 Myo9a$^{-/-}$ (G) compared with WT animals (H). The ventral caudal 3rd ventricle (*) and the rostral aqueduct (double arrowheads) are stenosed. ra, rostral aqueduct; ma, median aqueduct; ca, caudal aqueduct. Scale bars, 1 mm. (I) Coronal H&E-stained sections from P1.5 Myo9a$^{-/-}$ mutant brains show dilation of the ventral 3rd ventricle (arrowhead) due to partial stenosis of the ventral caudal 3rd ventricle (arrows) compared with the WT littermate control. Scale bar, 200 μm. (J) Stenosis of the aqueduct and denudation of the ependymal epithelial layer at restricted sites in P0.5 Myo9a$^{-/-}$ brains but not in the WT littermate control. Notably, closure of the third ventricle often precedes closure of the aqueduct, which becomes detectable at P0.5–P14.5. Scale bar, 100 μm. Quadrangles indicate enlarged areas in K and L showing denudation of the ependyma in Myo9a$^{-/-}$ brains. Scale bar, 20 μm.

earity index" (Otani *et al.*, 2006). These measurements confirmed that the cell boundaries depicting cell shape were less linear (Figure 3G). These differences were noted starting from P0.5. The single layer of ependymal epithelial cells was transformed at multiple sites along the ventral caudal 3rd ventricle and the aqueduct into a multilayer configuration (Figure 3, H–O). Cells that expressed the S100 marker protein for mature ependymal epithelial cells became disordered and part of amorphous accumulations of cells that obstructed the narrow ventricular passage (Figure 3M). Cell proliferation was not enhanced and could be excluded as a cause for the observed stenosis and closure of the ventricular system (Supplementary Figure S2).

Analysis of the tight junctions in morphologically still intact ependyma of the ventral caudal 3rd ventricle and the aqueduct of P0.5 Myo9a$^{-/-}$ mice revealed that staining for the protein occludin, a component of tight junctions, was reduced in the ventral caudal 3rd ventricle, was not detectable in large areas of the aqueduct, but was present in these regions in WT mice (Figure 4, A–D). The occludin staining was still preserved in the dorsal part of the aqueduct (Figure 4C). No alterations in the occludin staining were observed between Myo9a$^{-/-}$ and WT mice in ventricular regions that fully differentiate not till later in development. Also in the epithelium of the choroid plexus and the endothelium of blood vessels the occludin staining was similar in Myo9a$^{-/-}$ compared with WT tissue (Figure 4, E–H). The differences that were noted in the staining for occludin were not observed for the protein JAM-A, another component associated with tight junctions (data not shown). These results indicate that in the ependyma of Myo9a RhoGAP-deficient mice the molecular composition of tight junctions is altered sequentially in specific regions of the ventricular system. These specific regions coincide with the first ones to exhibit mature ependymal epithelial cells.

Myo9a Deficiency Reduces Ependymal Cell Maturation in the Ventral Caudal 3rd Ventricle and the Aqueduct

Ependymal cells mature at different times during development depending on where they are located in the ventricular system. They mature first in the very narrow regions such as the ventral part of the rostral aqueduct and the ventral

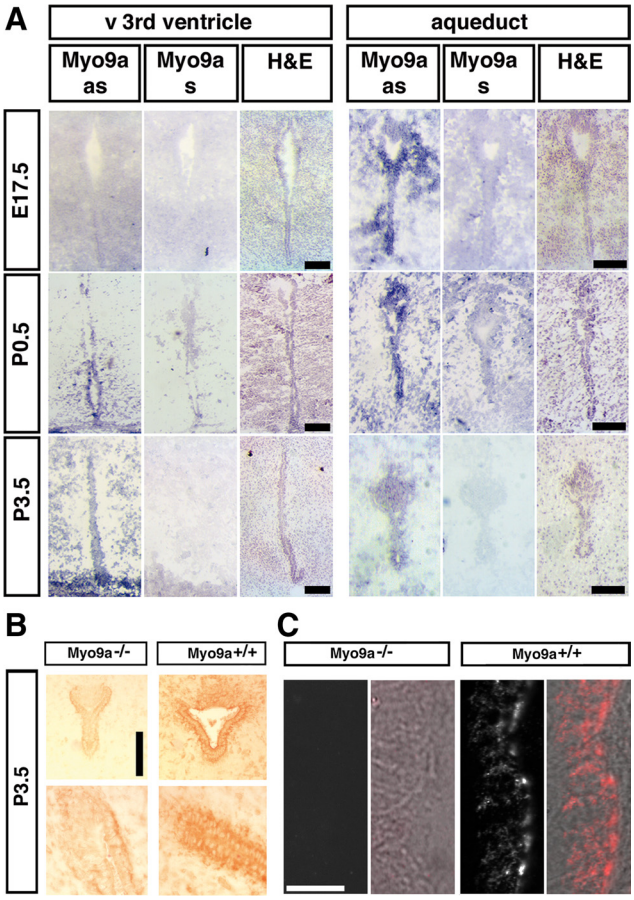

Figure 2. Myo9a is expressed in the maturing and fully differentiated ependyma. (A) In situ RNA hybridizations in E17.5, P0.5, and P3.5 WT brains showed strong Myo9a expression; as, Myo9a antisense (blue stain) in the ependymal cell layer lining the 3rd ventricle (left) and the aqueduct (right) connecting the 3rd and 4th ventricles in P0.5 and P3.5 mice. Myo9a expression was also detectable in the aqueduct of E17.5 embryos but not in the ventral 3rd ventricle. Corresponding WT brain tissue probed with a sense riboprobe (Myo9a s) never showed reactivity. Scale bars, 50 μm. (B) Immunohistochemical detection of Myo9a expression in P3.5 ependymal cell layer and aqueduct using an affinity-purified rabbit-anti-Myo9a antibody (Tü78). Myo9a protein is strongly expressed (brown color) in the ependymal cell layer and more weakly expressed in surrounding brain tissue of the 3rd ventricle (right, bottom) and aqueduct (right, top) of P3.5 mice. In the Myo9a$^{-/-}$ mutant little unspecific staining is observed in ependymal cells. Bar, 100 μm. (C) Confocal images of the ependyma in the aqueduct at P3.5 stained for Myo9a using an affinity-purified rabbit anti-Myo9a antibody (Tü78). Fluorescence images and corresponding DIC images overlaid with fluorescence image (red) are shown. Scale bar, 10 μm.

caudal 3rd ventricle at about E18 till birth (Silva-Alvarez *et al.*, 2005). Development of multiple cilia on the apical surface and proper ciliary beating are important to prevent hydrocephalus and stenosis (Ibañez-Tallon *et al.*, 2004; Lechtreck *et al.*, 2008). Using the marker protein S100 and a marker for cilia to identify mature ependymal cells, we found that at P0.5 the number of mature ependymal cells in the ventral caudal 3rd ventricle and the rostral aqueduct was reduced in Myo9a$^{-/-}$ cells compared with WT cells (Figure 5; Supplementary Figure S3A). We quantified the total number of ependymal cells and the number of cells that were multiciliated and positive for S100 in the ventral part of the rostral aqueduct. Although the total number of ependymal cells was slightly reduced in Myo9a$^{-/-}$ ependyma compared with WT (72 $\pm$ 10.4, n = 4 and 88.5 $\pm$ 11.9, n = 5, respectively), the number of S100-positive (34.7 $\pm$ 5.6 and 68.9 $\pm$ 17.8%, respectively) and multiciliated ependymal cells (34.4 $\pm$ 7.4 and 62 $\pm$ 15.4%, respectively) was significantly reduced ($p < 0.05$; Figure 5C). Independent of the genotype, ~95% of all ependymal cells positive for S100 were also multiciliated (Supplementary Figure S3B). The ~50% reduced number of multiciliated ependymal cells in the rostral aqueduct of Myo9a$^{-/-}$ compared with WT mice may reduce the flow of CSF. The number of multiciliated and S100-positive ependymal cells was similarly reduced in the caudal ventral 3rd ventricle of Myo9a$^{-/-}$ mice (Supplementary Figure S3A).

Oral Administration of the ROCK-Inhibitor Y-27632 Diminishes Lateral Ventricle Enlargement in Myo9a-deficient Mice and Restores Ependymal Cell Maturation

The RhoGAP domain of Myo9a specifically inactivates Rho A, B, and C (Chieregatti *et al.*, 1998). An important effector of the Rho proteins is ROCK. To test for a potential role of increased Rho-ROCK signaling in hydrocephalus formation in Myo9a-deficient mice, we administered the ROCK-inhibitor Y-27632 orally in the drinking water during late embryonic and early postnatal development. The area occupied by the lateral ventricles in comparison to the total brain section area was determined in mice at age P3.5 (Figure 6). The ratio determined for the WT mice treated with vehicle was set to 100 $\pm$ 14.3% (n = 18). The size of the lateral ventricles of WT mice treated with ROCK-inhibitor did not differ significantly from mice treated with vehicle (93.5 $\pm$ 17.7%, n = 18). Myo9a$^{-/-}$ mice exhibited significantly enlarged lateral ventricles when treated with vehicle (401.5 $\pm$ 57.9%, n = 18, $p < 0.01$), but no longer when treated with ROCK-inhibitor (220 $\pm$ 36.7%, n = 20; Figure 6).

To test for a genetic interaction of Myo9a with Rho proteins in hydrocephalus formation, we were only able to obtain mice deficient for RhoB. Mice deficient for RhoB are fertile and exhibit no obvious phenotype (Liu *et al.*, 2001). To investigate a possible genetic interaction between the RhoGAP Myo9a and RhoB, we generated compound mutant mice deficient in the functions of both proteins. Compound mutant Myo9a$^{-/-}$;RhoB$^{-/-}$ mice were born at Mendelian ratio but failed to show rescue of aqueduct stenosis by P21.5 (Supplementary Figure S4), indicating that deletion of RhoB does not attenuate hydrocephalus formation in Myo9a-deficient mice.

To address the molecular mechanism by which ROCK-inhibitor attenuates lateral ventricle enlargement, we determined the number of mature S100-protein–positive cells in the ventral part of the rostral aqueduct at P3 in WT and Myo9a-deficient mice that were treated with Y-27632. No differences were observed in the number of ependymal cells that express the S100 protein (Figure 7, A and B). This is unlike in mice not treated with Y-27632, which showed a significantly reduced number of S100-positive cells when deficient for Myo9a. Therefore, the administration of ROCK-inhibitor rescues the maturation of ependymal cells in Myo9a-deficient mice. However, it did not rescue the altered cell morphology (Figure 7C). The distribution of occludin in tight junctions could not be assessed reliably as treatment with ROCK-inhibitor impaired the localization of occludin in WT mice.

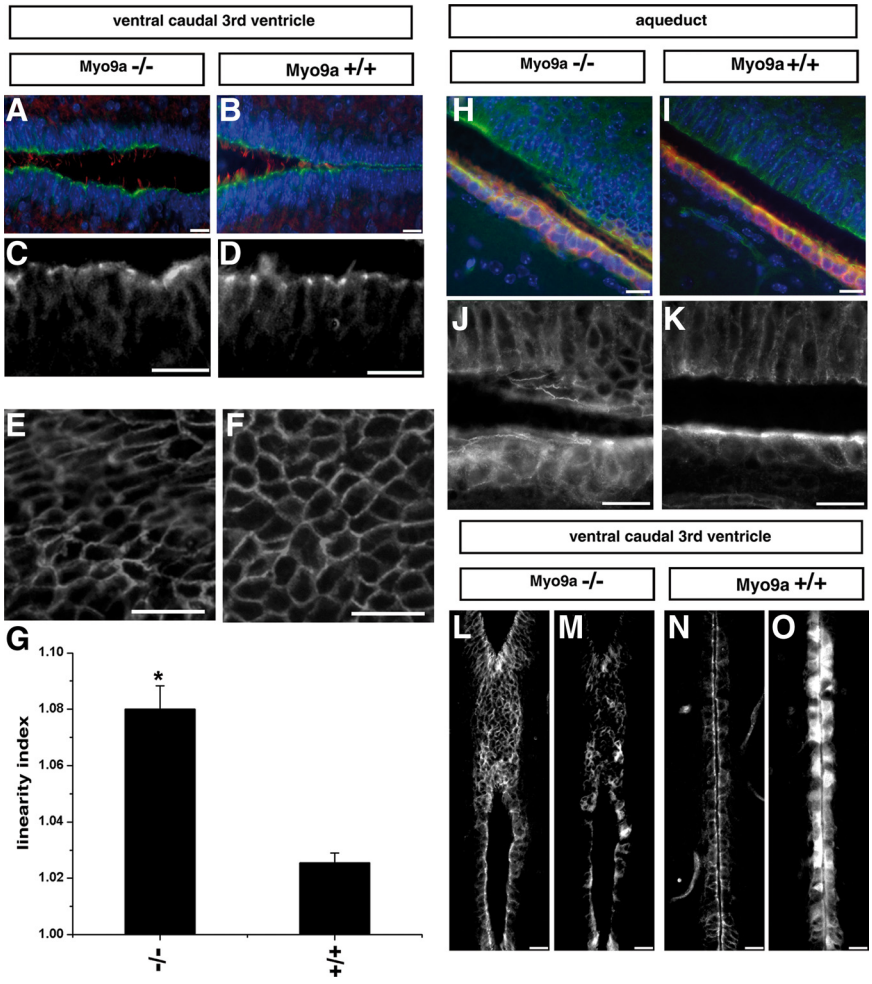

Figure 3. Loss of Myo9a causes altered ependymal cell shape and distorts the ependymal epithelium in the ventral caudal 3rd ventricle and the aqueduct. (A and B) Double immunofluorescence staining of coronal sections from P0.5 Myo9a$^{-/-}$ (A) and WT littermate mice (B) with anti-E-cadherin (green; adherens junction marker), anti-acetylated tubulin (red; cilia marker), and DAPI showing distortion of the ependymal layer of the ventral caudal 3rd ventricle in Myo9a$^{-/-}$ mice compared with WT mice. Note the presence of apical cilia despite a distorted structure of the ependyma in Myo9a$^{-/-}$ mice (A). (C and D) Enlargement of selected areas from A and B, respectively, stained for E-cadherin, highlighting the distortion of the ependyma. (E and F) Immunofluorescence staining of sagittal sections from P3.5 Myo9a$^{-/-}$ and WT littermate mice with anti-β-catenin (adherens junction marker) showing the irregular cell shape of the ependymal cells and the distortion of the ependymal cell layer in Myo9a$^{-/-}$ mice. (G) Quantification of junction linearity in the ependymal epithelium. In sections stained for β-catenin junction length and the distance between vertices were measured to determine the linearity index that is defined by the ratio of junction length to the distance between vertices. This index is significantly increased in Myo9a$^{-/-}$ mice. *$p < 0.05$, $n = 2$ mice of each genotype. Several areas of 100 μm $\times$ 100 μm were analyzed with more than 100 cells in total from each genotype. (H and I) Staining of sagittal sections of the aqueduct from P3.5 Myo9a$^{-/-}$ (H) and WT littermate mice (I) with anti-β-catenin (green) and anti-S100 (red, marker of mature ependymal cells) showing stenosis, distortion, and multilayer formation of the ependyma in the aqueduct in Myo9a$^{-/-}$ mice. (J and K) Enlargements of selected areas in H and I, respectively, stained for β-catenin. (L–O) Coronal sections of partially fused ventral caudal 3rd ventricle stained for β-catenin (L and N) and S100 protein (M and O). Scale bars, 20 μm.

Myo9a Regulates Epithelial Differentiation of Caco-2 Cells and Junction-associated Signaling

We next used a tissue culture model to analyze the role of Myo9a in epithelial differentiation with the aims to determine whether the protein is also of functional relevance in nonependymal epithelia and to start to analyze its functional role on a cellular level. We used the human adenocarcinoma cell line Caco-2, a well-established model to analyze epithelial differentiation (Pinto *et al.*, 1983; Hauri *et al.*, 1985). Transient transfection of siRNA was used to knockdown Myo9a expression in Caco-2 cells. Figure 8A shows that Myo9a was efficiently depleted by specific siRNAs but not by nontargeting or control siRNAs. We have used two different pools of Myo9a-specific siRNAs that gave similar results (see *Materials and Methods*; only results with ON-TARGETplus siRNAs are shown). To test if depletion of Myo9a induces an increase in Rho-signaling, we monitored the amount of phosphorylated myosin light-chain phosphatase, a substrate of ROCK, by immunoblotting with antibodies specific for the phosphorylated form (Figure 8B). The amount of phosphorylated myosin light-chain phosphatase was increased in Caco-2 cells depleted for Myo9a to 1.45 (SD 0.11, $n = 4$, $p = 0.001$; *t* test) of the value determined in Caco-2 cells treated with control siRNA, indicating that Rho-activity was up-regulated.

Myo9a-deficiency caused ependymal cells to fail to differentiate normally and led to irregular cell shapes and an apparent reduction in junctional association of occludin. Hence, we first tested expression of various tight junction proteins as well as β-catenin in Caco-2 cells with reduced expression of Myo9a. However, no differences between control and Myo9a-depleted cells were observed, indicating that depletion of Myo9a does not lead to a general reduction in tight junction protein expression (Supplementary Figure S5).

To determine where in Caco-2 cells Myo9a is localized and might act, we studied its distribution by immunofluorescence microscopy (Figure 8, C and D). Myo9a antibody staining was observed along cell–cell junctions and in the cytosol. Depletion of Myo9a abolished junctional staining and only slightly reduced cytosolic staining. This validated the specificity of the junctional staining. The junctional staining for Myo9a neither showed a perfect colocalization with adherens junctions nor with tight junctions (Figure 8D), suggesting a broader distribution over the junctional complex.

We next used immunofluorescence to analyze effects on differentiation and junction formation. Figure 8E shows that Myo9a depletion led to reduced staining of the apical marker DPPIV, a protein whose expression levels are differentiation dependent (Hauri *et al.*, 1985). Moreover, staining

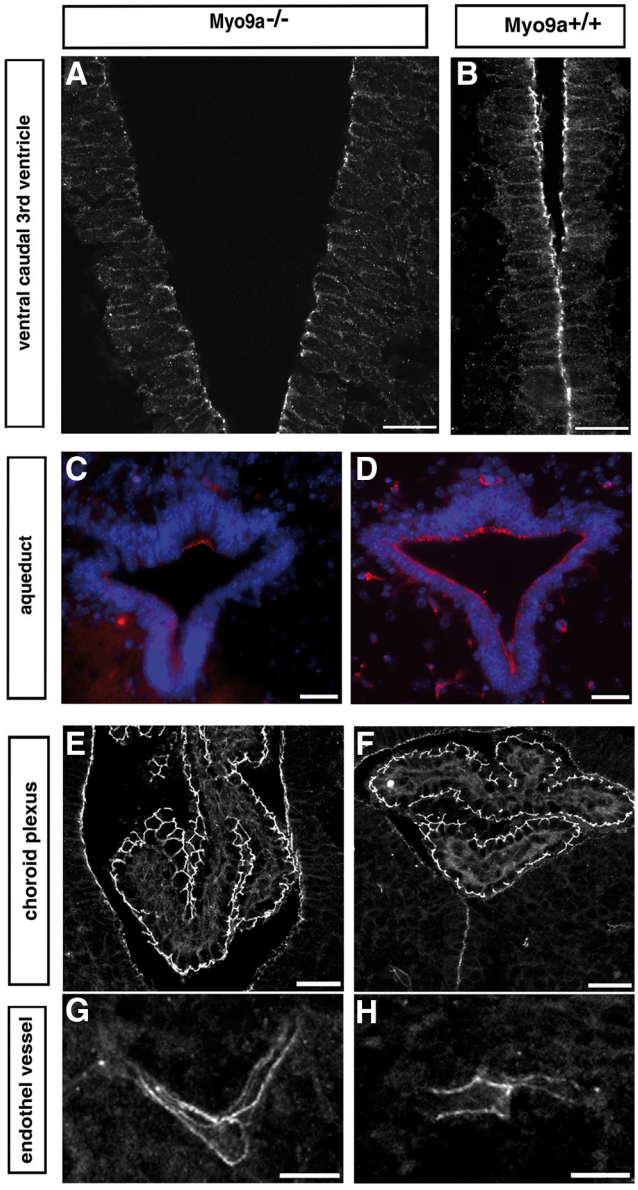

Figure 4. Occludin staining is decreased in tight junctions of ependymal epithelium of the ventral caudal 3rd ventricle and the aqueduct, but not in the epithelium of the choroid plexus or the endothelium lining the blood vessels. Immunofluorescence staining of coronal sections from P0.5 Myo9a$^{-/-}$ (A, C, E, and G) and WT littermate mice (B, D, F, and H) for occludin showing that it is reduced in tight junctions of the ependyma in the ventral caudal 3rd ventricle (A) and the aqueduct (C, red) from Myo9a$^{-/-}$ mouse brains. No difference in occludin staining was observed in the epithelium of the choroid plexus (E and F) and the endothelium lining the blood vessels (G and H) in Myo9a$^{-/-}$ compared with control tissue. Scale bars, (A and B) 20 μm; (C–H) 30 μm.

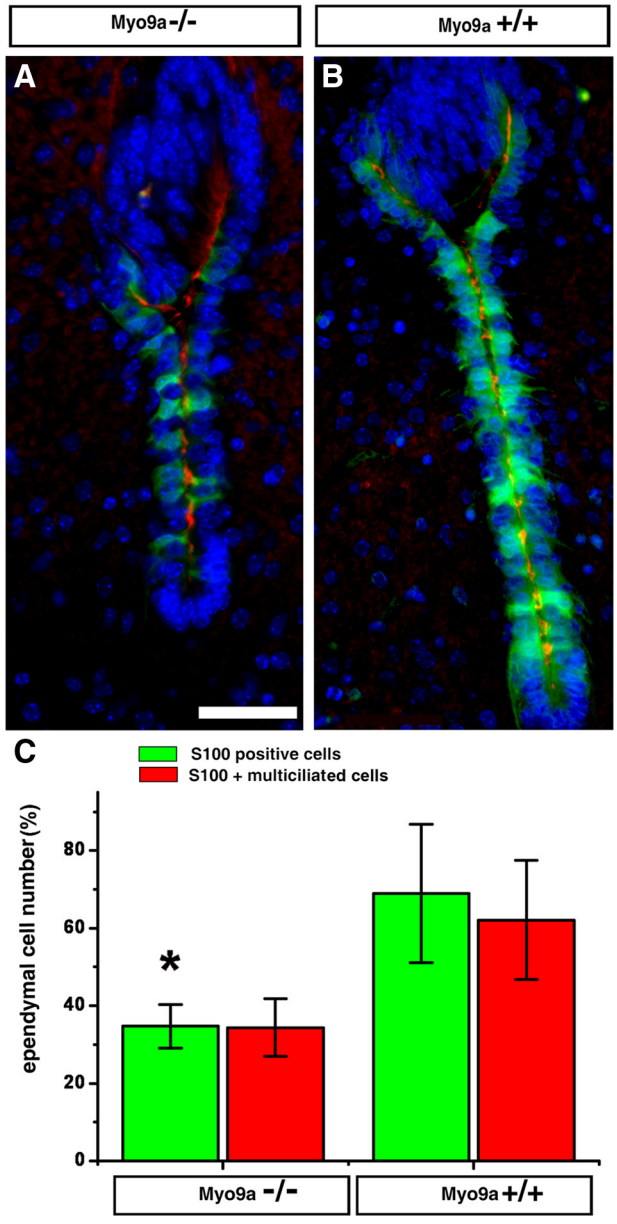

Figure 5. Myo9a deficiency decreases the number of S100 protein positive, multiciliated ependymal cells in the aqueduct. (A and B) Immunofluorescence staining of coronal sections from P0.5 Myo9a$^{-/-}$ (A) and WT mice (B) for S100 protein (green), acetylated tubulin (red), and DNA (blue). (C) Statistical analysis of S100-positive and multiciliated ependymal cells. The number of S100-positive ependymal cells was reduced in Myo9a$^{-/-}$ mice (34.7 $\pm$ 5.6%; n = 4) compared with Myo9a$^{+/+}$ mice (68.9 $\pm$ 17.8%; n = 5; *p $<$ 0.05). The number of multiciliated ependymal cells was similarly reduced (34.4 $\pm$ 7.4 vs. 62 $\pm$ 15.4%). Scale bar, 50 μm.

for NaK-ATPase, a basolateral membrane protein, revealed that the cells had lost their regular shape and appearance. Staining for tight (ZO-1, occludin, ZO-2, claudin-1) and adherens (β-catenin, E-cadherin) junction proteins further supported this conclusion because the cells appeared more flattened and, hence, larger. Nevertheless, junctional accumulation of all tested proteins still occurred, suggesting that intercellular junctions could still assemble. Nevertheless, the junctional staining appeared weaker in Myo9a-depleted cells and, in some cases, there was considerable cytosolic staining (e.g., ZO-2; β-catenin). Although these observations suggest that junction formation is compromised in Myo9a-depleted cells, a more detailed analysis will require stable knockdown cell lines.

The interference of Myo9a depletion with Caco-2 cell differentiation was suggestive of changes in gene expression. Therefore, we analyzed transcriptional activities regulated by different signaling pathways using reporter assays. Rho-signaling activates the transcription factor SRF that binds

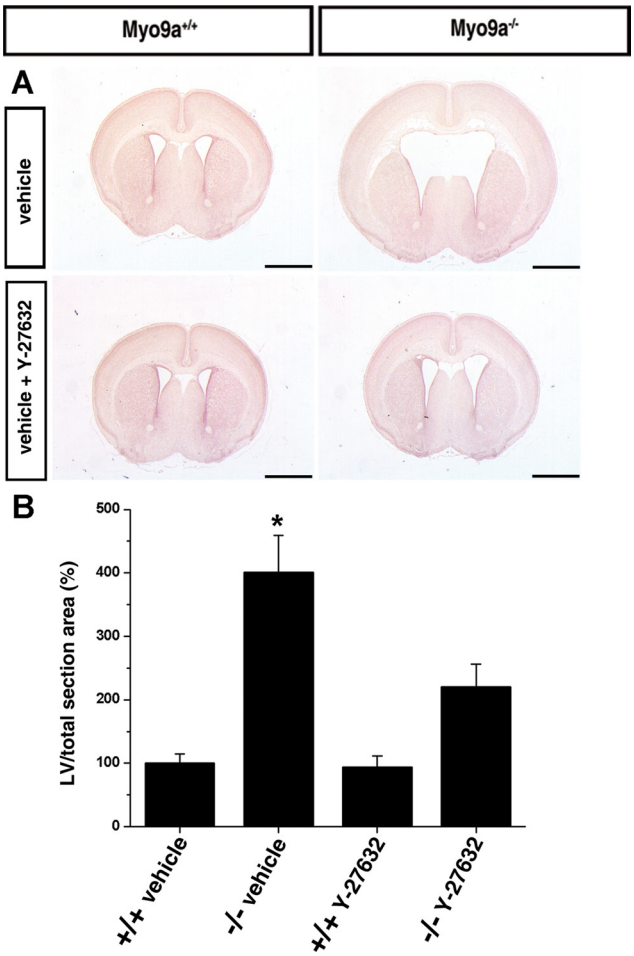

Figure 6. Hydrocephalus formation in Myo9a-deficient mice is attenuated by the inhibition of Rho-dependent kinase. (A and B) Oral administration of ROCK-inhibitor Y-27632 to pregnant mice attenuates hydrocephalus formation in newborns. (A) Representative H&E-stained coronal brain sections from vehicle control groups ($Myo9a^{+/+}$, n = 18; $Myo9a^{-/-}$, n = 18) that were maintained on tap water with sucrose (30% vol/wt) and from Y-27632 groups ($Myo9a^{+/+}$, n = 18; $Myo9a^{-/-}$, n = 20) that were maintained on tap water with Y-27632 (200 mg/l) and sucrose (30% vol/wt). The two groups were treated from E12.5 until P3.5. Bars, 1 mm. (B) Morphometric analysis. The ratio of the area covered by the lateral ventricle in a defined brain area (at the anterior commissure) to the total brain section area was determined and set to 100% in the control groups. Treatment of $Myo9a^{-/-}$ mice with Y-27632 ROCK-inhibitor significantly (*$p < 0.01$) attenuates LV enlargement.

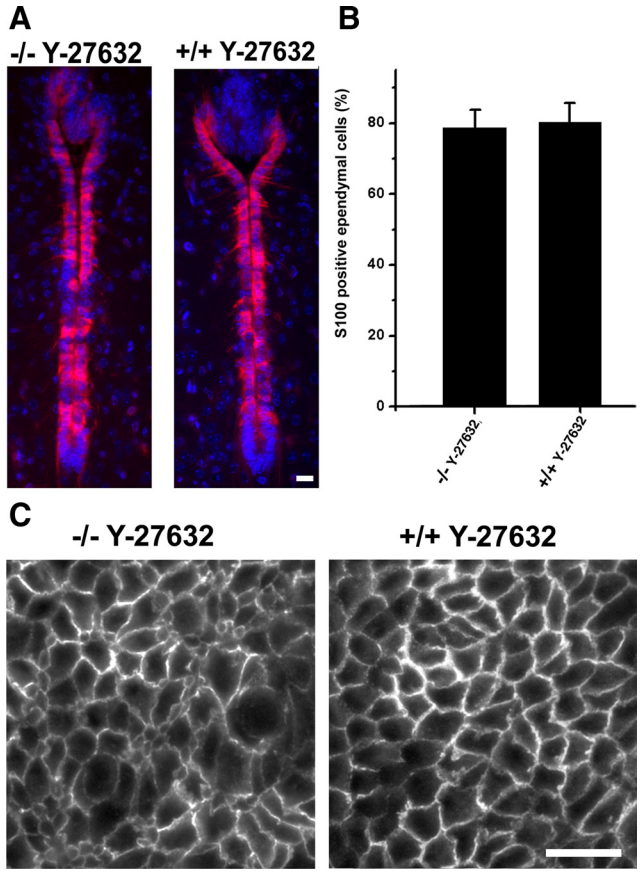

Figure 7. Administration of ROCK-inhibitor Y-27632 rescues ependymal cell maturation, but not ependyma morphology. (A and B) Ependymal cells in the aqueduct of P3.5 $Myo9a^{-/-}$ and WT ($Myo9a^{+/+}$) mice treated with ROCK inhibitor Y-27632 were stained for S100 protein (red), a marker of mature ependymal cells (A). Cell nuclei were stained with DAPI (blue). Scale bar, 20 μm. (B) Statistical analysis of S100-positive ependymal cells in the aqueduct of P3.5 $Myo9a^{-/-}$ and WT mice treated with Y-27632. No difference in numbers of mature ependymal cells could be detected. Five mice of each genotype were analyzed. (C) Cross sections of the ependyma in the aqueduct of P3.5 $Myo9a^{-/-}$ and WT ($Myo9a^{+/+}$) mice treated with Y-27632. Sections were stained for β-catenin to visualize cell–cell junctions. Scale bar, 20 μm.

SREs. Compared with cells treated with control siRNA, the SRE-mediated transcription was increased in cells depleted of Myo9a (Figure 8F). This result is indicative of increased Rho-signaling. Rho-signaling has also been reported to activate transcription by NF-κB. Depletion of Myo9a also increased the activity of NF-κB (Figure 8G). When cells were treated simultaneously with the Rho-inhibitor C3 transferase, the transcriptional activity of NF-κB did not differ between cells that were or were not depleted of Myo9a (Figure 8G), suggesting that NF-κB activation was at least partially mediated by increased Rho signaling.

Myo9a depletion resulted in reduced junction assembly and the appearance of nuclear β-catenin staining; hence, we next measured the effect on gene expression pathways regulated by cell–cell junctions. We first measured signaling by β-catenin using a luciferase reporter assay to measure the transcriptional coactivation activity of β-catenin (van de Wetering *et al.*, 1997). Figure 8H shows that knockdown of Myo9a indeed stimulated expression of luciferase driven by a reporter with functional TCF-binding sites but not if expression of the reporter was driven by a control promoter lacking such binding sites. Depletion of Myo9a thus resulted in the activation of β-catenin/TCF-driven transcription, suggesting that the observed defects in differentiation might at least in part be caused by aberrant β-catenin signaling.

Epithelial tight junctions also influence transcription. They regulate the activity of the Y-box factor ZONAB whose activity can also be analyzed with a luciferase-based assay (Balda and Matter, 2000; Frankel *et al.*, 2005). Figure 8I shows that ZONAB's transcriptional activity was reduced by Myo9a depletion, suggesting that Myo9a depletion differentially affects signaling pathways that are regulated by intercellular junctions. As ZONAB is normally activated by increased Rho signaling (Nie *et al.*, 2009), this suggests that Myo9a depletion also exerts Rho-independent effects. This is

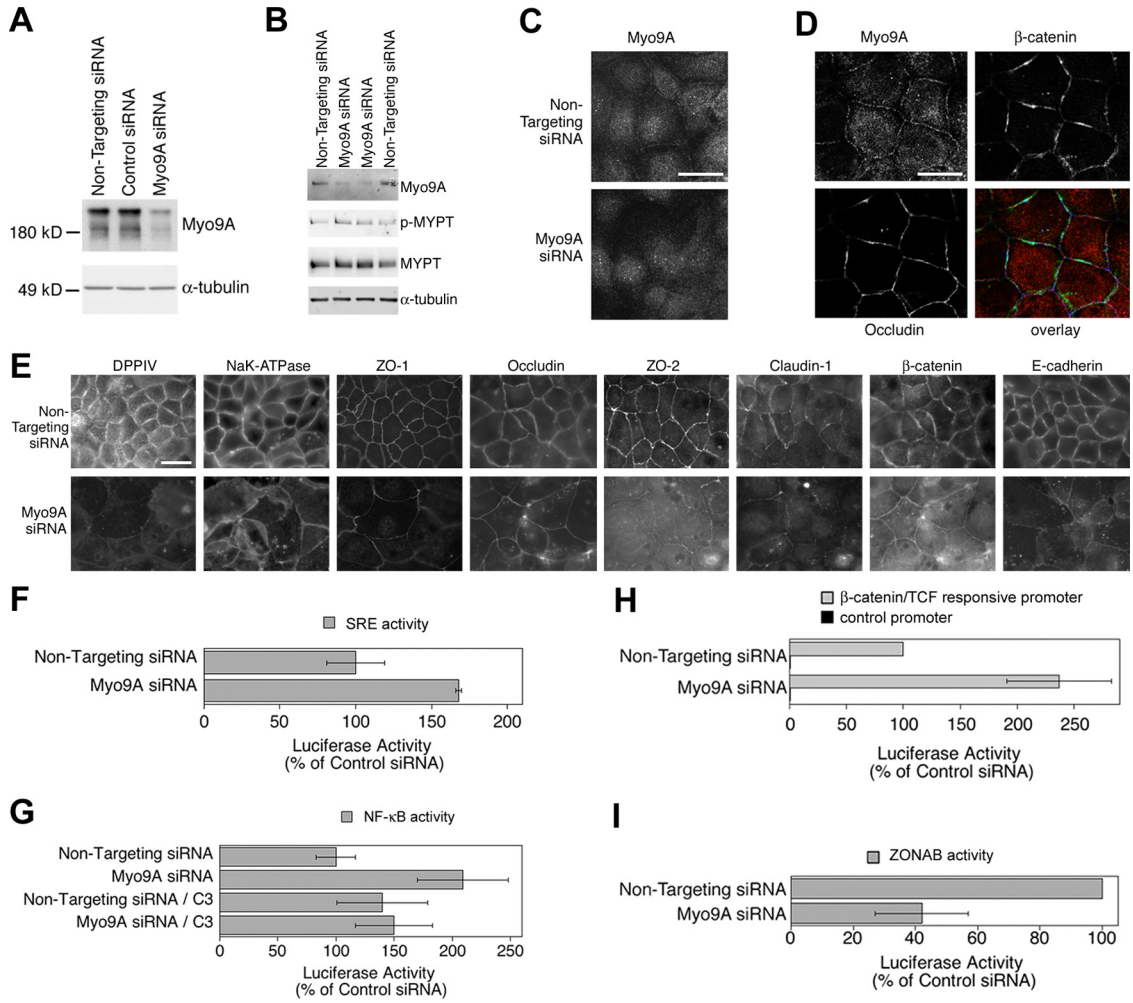

Figure 8. Depletion of Myo9a in Caco-2 cells alters cell morphology, differentiation, Rho-signaling and junctional signaling. (A) Caco-2 cells were transfected with control and Myo9a-targeting siRNAs. After 72 h, the cells were lysed, and expression of Myo9a was analyzed by immunoblotting total cell extacts. α-Tubulin was used as a loading control. (B) Samples of cells treated either with control or Myo9a-targeting siRNAs were analyzed by immunoblotting for the amount of phosphorylated (p-MYPT) and total myosin light chain phosphatase (MYPT). α-Tubulin served as a loading control. (C) Indirect immunofluorescence staining for Myo9a in cells treated with control or Myo9a-targeting siRNAs. Note the disappearance of the junctional staining in cells treated with Myo9a-targeting siRNA. Epifluorescence images; scale bar, 10 μm. (D) The junctional staining of Myo9a does not discriminate between tight and adherence junctions. Confocal sections were taken at the level of the junctions. Caco-2 cells were simultaneously stained for Myo9a, β-catenin, and occludin. Individual stainings and an overlay of the three stainings are shown. Scale bar, 10 μm. (E) Caco-2 cells were transfected with siRNAs as in A and were then fixed and processed for immunofluorescence. Shown are images for the apical marker DPPIV, the basolateral marker NaK-ATPase as well as a set of tight and adherens junction proteins. (F) Transcriptional activity of a reporter plasmid with SRE-dependent luciferase expression. Values obtained with nontargeting siRNAs were set to 100%. (G) Transcriptional activity of NF-κB as measured with a reporter plasmid harboring functional NF-κB-binding sites. Activities were determined in the absence and presence of the Rho-inhibitor C3 transferase (C3). (H and I) Transcriptional activities of β-catenin/TCF and ZONAB, respectively, were measured using luciferase reporter assays. For β-catenin/TCF, results obtained with a reporter plasmid with functional TCF-binding sites as well as with one lacking such sites are shown. For ZONAB, plasmids harboring a promoter with a ZONAB-binding site driving firefly luciferase expression and a promoter with an inactivated binding site but otherwise identical sequence driving renilla luciferase were cotransfected, and the resulting ratios were used to calculate ZONAB activity. Values obtained with nontargeting siRNAs were set to 100%. Values are means ± SD derived from three experiments performed in triplicates.

also supported by the observation that neither the effect on ZONAB nor on β-catenin–regulated transcription could be blocked with C3 transferase (unpublished observations).

DISCUSSION

Congenital hydrocephalus affects one to three humans per 1000 live births. In the present study, we report that mice deficient for the Myo9a exhibit alterations in morphology and differentiation of the ependymal epithelium and develop hydrocephalus. The caudal region of the ventral 3rd ventricle and the aqueduct show stenosis or closures that block the flow of CSF. It is precisely in these two narrow ducts that the ependymal epithelial cells mature first during development and become multiciliated (Silva-Alvarez *et al.*, 2005; Spassky *et al.*, 2005). This might be related to the fact that the flow of CSF in narrow regions of the ventricular system has to be faster than in wider regions. Ciliary beating might provide for a faster flow of CSF. Indeed, compromised ciliary beating has been shown to cause hydroceph-

alus (Ibañez-Tallon *et al.*, 2004; Marshall and Nonaka, 2006; Lechtreck *et al.*, 2008; Town *et al.*, 2008). Therefore, the reduced numbers of mature multiciliated ependymal cells could be causally related to the development of hydrocephalus in mice deficient for Myo9a. This notion is supported by the finding that ventricular enlargement was significantly attenuated in Myo9a-deficient mice that had been treated with ROCK-inhibitor Y-27632. Administration of ROCK-inhibitor Y-27632 restored ependymal cell maturation resulting in a normal number of multiciliated cells. Furthermore, this result implies that the down-regulation of Rho-ROCK signaling by the RhoGAP Myo9a is important for ependymal cell differentiation. Cell maturation or differentiation is regulated by gene expression. In epithelial Caco-2 cells that were depleted of Myo9a defects in differentiation and alterations in various transcriptional activities could be demonstrated. These cells exhibited among others increased SRE and NF-κB activities due to enhanced Rho-signaling. Both SRF and NF-κB signaling have been implicated in differentiation.

Myo9a was located at cell junctions where it might subserve its functions. Epithelial cell junctions are critical regulators of gene expression (Matter *et al.*, 2005; Matter and Balda 2007). They control the activity of transcription factors that can interact with junctional components. We noted that tight junctions in the ependyma were modified in the absence of Myo9a and contained a reduced amount of the transmembrane protein occludin. Alterations in junctional assembly were also noted in Caco-2 cells with a knockdown of Myo9a. The observed differences in transcriptional activity of β-catenin and ZONAB in Caco-2 Myo9a knockdown cells were likely due to alterations in junctional assembly. These two proteins can interact with junctional components, which inhibits their nuclear functions.

β-Catenin is a component of the adherens junctions and the canonical Wnt signaling pathway (Grigoryan *et al.*, 2008; Schlessinger *et al.*, 2009). It has been shown together with Lef-1 to interact with PITX2 and synergistically regulate the promoter of the transcription factor FoxJ1 (HFH-4; Venugopalan *et al.*, 2008). FoxJ1 is regulating the differentiation of epithelia with motile cilia and its absence induces hydrocephalus (Chen *et al.*, 1998; Brody *et al.*, 2000). Further evidence that increased β-catenin signaling might contribute to hydrocephalus formation in Myo9a-deficient mice is provided by the finding of a genetic interaction between the adenomatous polyposis coli (APC) protein and Lis1. APC inhibits β-catenin activity, whereas Lis1 is an effector in the reelin signaling pathway (Assadi *et al.*, 2003). The presence of a mutant APC allele increased the incidence of hydrocephalus in Lis+/− mice (Hebbar *et al.*, 2008).

Likewise, changes in the transcriptional activity of ZONAB might contribute to hydrocephalus formation in Myo9a-deficient mice. ZONAB interacts with the RNA-processing factor symplekin (Kavanagh *et al.*, 2006). The down-regulation of symplekin expression reduces transcriptional activity of ZONAB. Symplekin has also been shown to interact with the transcription factor HSF-1 in response to heat shock (Xing *et al.*, 2004). Interestingly, HSF-1 null mice were reported to exhibit a mild hydrocephalus (Takaki *et al.*, 2007). These findings demonstrate that the deficiency of Myo9a aside from Rho-signaling impinges on several other signaling pathways that might contribute to hydrocephalus formation. How these different signaling pathways are connected with Myo9a, and the determination of their individual contributions to hydrocephalus formation are interesting topics for further studies.

Tight and adherens junctions are intimately linked with the actin cytoskeleton. Rho-signaling is known to regulate the actin cytoskeleton and cell contractility (Jaffe and Hall 2005). Therefore, it was not unanticipated to find that the deficiency in Myo9a perturbed ependymal cell morphologies. Acto-myosin II contraction can lead to increased epithelial permeability and endocytosis of occludin (Hecht *et al.*, 1996; Turner *et al.*, 1997; Utech *et al.*, 2005; Shen *et al.*, 2006). Interestingly, administration of ROCK-inhibitor that is expected to down-regulate acto-myosin II contraction did not modify the altered ependymal cell morphologies. This observation suggests that possibly additional Rho-effectors or potential Rho-independent functions of Myo9a control ependymal cell morphology.

The demonstration that hydrocephalus formation in mice can be attenuated by a ROCK-inhibitor suggests that a similar therapeutic intervention might also be promising for some of the human cases of hydrocephalus. The inhibition of ROCK with the ROCK-inhibitor Y-27632 had no obvious adverse effects in mice. Administration of the ROCK-inhibitor fasudil to humans with subarachnoid hemorrhage was well tolerated (Suzuki *et al.*, 2007, 2008), indicating that treatment of humans with ROCK-inhibitors might be feasible.

ACKNOWLEDGMENTS

B. Terstegge, P. Nikolaus, M. Müller, and A. Freitag provided skillful technical assistance. We acknowledge the generous gifts of antibody C3B9 from K. Gull (Oxford), Jam A antibodies from K. Ebnet (Münster), and RhoB-deficient mice from G. C. Prendergast (Philadelphia). This work was supported by a grant of the Deutsche Forschungsgemeinschaft SFB629/A2 and the Wellcome Trust (084678/Z/08/Z).

REFERENCES

Aijaz, S., D'Atri, F., Citi, S., Balda, M. S., and Matter, K. (2005). Binding of GEF-H1 to the tight junction-associated adaptor cingulin results in inhibition of Rho signaling and G1/S phase transition. Dev. Cell *8*, 777–786.

Assadi, A. H., *et al.* (2003). Interaction of reelin signalling and Lis1 in brain development. Nat. Genet. *3*, 270–276.

Bähler, M. (2008). Class IX myosins. In: Myosins, ed. L. M. Coluccio, Netherlands: Springer, 391–401.

Balda, M. S., and Matter, K. (2003). Epithelial cell adhesion and the regulation of gene expression. Trends Cell Biol. *13*, 310–318.

Balda, M. S., Garrett, M. D., and Matter, K. (2003). The ZO-1-associated Y-box factor ZONAB regulates epithelial cell proliferation and cell density. J. Cell Biol. *160*, 423–432.

Balda, M. S., and Matter, K. (2000). The tight junction protein ZO-1 and an interacting transcription factor regulate ErbB-2 expression. EMBO J. *19*, 2024–2033.

Balda, M. S., Whitney, J. A., Flores, C., González, S., Cereijido, M., and Matter, K. (1996). Functional dissociation of paracellular permeability and transepithelial electrical resistance and disruption of the apical-basolateral intramembrane diffusion barrier by expression of a mutant tight junction membrane protein. J. Cell Biol. *134*, 1031–1049.

Banizs, B., Pike, M. M., Millican, C. L., Ferguson, W. B., Komlosi, P., Sheetz, J., Bell, P. D., Schwiebert, E. M., and Yoder, B. K. (2005). Dysfunctional cilia lead to altered ependyma and choroid plexus function, and result in the formation of hydrocephalus. Development. *132*, 5329–5339.

Benais-Pont, G., Punn, A., Flores-Maldonado, C., Eckert, J., Raposo, G., Fleming, T. P., Cereijido, M., Balda, M. S., and Matter, K. (2003). Identification of a tight junction-associated guanine nucleotide exchange factor that activates Rho and regulates paracellular permeability. J. Cell Biol. *160*, 729–740.

Bernards, A. (2003). GAPs galore! A survey of putative Ras superfamily GTPase activating proteins in man and *Drosophila*. Biochim. Biophys. Acta *1603*, 47–82.

Brody, S. L., Yan, X. H., Wuerffel, M. K., Song, S-K., and Shapiro, S. D. (2000). Ciliogensis and left-right axis defects in forkhead factor HFH-4-null mice. Am. J. Respir. Cell. Mol. Biol. *23*, 45–51.

Chae, T. H., Kim, S., Marz, K. E., Hanson, P. I., and Walsh, C. A. (2004). The hyh mutation uncovers roles for alpha Snap in apical protein localization and control of neural cell fate. Nat. Genet. *36*, 264–270.

Chen, J., Knowles, H. J., Hebert, J. L., and Hackett, B. P. (1998). Mutation of the mouse hepatocyte nuclear factor/forkhead homologue 4 gene results in an absence of cilia and random left-right asymmetry. J. Clin. Invest. *102*, 1077–1082.

Chieregatti, E., Gärtner, A., Stöffler, H-E., and Bähler, M. (1998). Myr 7 is a novel myosin IX-RhoGAP expressed in rat brain. J. Cell Sci. *111*, 3597–3608.

De Vries, W. N., Binns, L. T., Fancher, K. S., Dean, J., Moore, R., Kemler, R., and Knowles, B. B. (2000). Expression of Cre recombinase in mouse oocytes: a means to study maternal effect genes. Genesis *26*, 110–112.

Fang, W. B., Ireton, R. C., Zhuang, G., Takahashi, T., Reynolds, A., and Chen, J. (2008). Overexpression of EPHA2 receptor destabilizes adherens junctions via a RhoA-dependent mechanism. J. Cell Sci. *121*, 358–368.

Frankel, P., Aronheim, A., Kavanagh, E., Balda, M. S., Matter, K., Bunney, T. D., and Marshall., C. J. (2005). RalA interacts with ZONAB in a cell density-dependent manner and regulates its transcriptional activity. EMBO J. *24*, 54–62.

Gorman, S. W., *et al.* (1999). The cloning and developmental expression of unconventional myosin IXA (MYO9A) a gene in the Bardet-Biedl syndrome (BBS4) region at chromosome 15q22-q23. Genomics *59*, 150–160.

Grigoryan, T., Wend, P., Klaus, A., and Birchmeier, W. (2008). Deciphering the function of canonical Wnt signals in development and disease: conditional loss- and gain-of-function mutations of β-catenin in mice. Genes Dev. *22*, 2308–2341.

Hauri, H. P., Sterchi, E. E., Bienz, D., Fransen, J. A., and Marxer, A. (1985). Expression and intracellular transport of microvillus membrane hydrolases in human intestinal epithelial cells. J. Cell Biol. *101*, 838–851.

Hebbar, S., Guillotte, A. M., Mesngon, M. T., Zhou, Q., Wynshaw-Boris, A., and Smith, D. S. (2008). Genetic enhancement of the Lis1+/− phenotype by a heterozygous mutation in the adenomatous polyposis coli gene. Dev. Neurosci. *30*, 157–170.

Hecht, G., Pestic, L., Nikcevic, G., Koutsouris, A., Tripuraneni, J., Lorimer, D. D., Nowak, G., Guerriero, V., Jr., Elson, E. L., and Lanerolle, P. D. (1996). Expression of the catalytic domain of myosin light chain kinase increases paracellular permeability. Am. J. Physiol. *271*, C1678–C1684.

Homem, C. C., and Peifer, M. (2008). Diaphanous regulates myosin and adherens junctions to control cell contractility and protrusive behavior during morphogenesis. Development *135*, 1005–1018.

Ibañez-Tallon, I., Pagenstecher, A., Fliegauf, M., Olbrich, H., Kispert, A., Ketelsen, U. P., North, A., Heintz, N., and Omran, H. (2004). Dysfunction of axonemal dynein heavy chain Mdnah5 inhibits ependymal flow and reveals a novel mechanism for hydrocephalus formation. Hum. Mol. Genet. *13*, 2133–2141.

Imai, F., Hirai, S., Akimoto, K., Koyama, H., Miyata, T., Ogawa, M., Noguchi, S., Sasaoka, T., Noda, T., and Ohno, S. (2006). Inactivation of aPKClambda results in the loss of adherens junctions in neuroepithelial cells without affecting neurogenesis in mouse neocortex. Development *133*, 1735–1744.

Jaffe, A. B., and Hall, A. (2005). Rho GTPases: biochemistry and biology. Annu. Rev. Cell Dev. Biol. *21*, 247–269.

Kavanagh, E., Buchert, M., Tsapara, A., Choquet, A., Balda, M. S., Hollande, F., and Matter, K. (2006). Functional interaction between the ZO-1-interacting transcription factor ZONAB/DbpA and the RNA processing factor symplekin. J. Cell Sci. *119*, 5098–5105.

Khelfaoui, M., *et al.* (2007). Loss of X-linked mental retardation gene oligophrenin1 in mice impairs spatial memory and leads to ventricular enlargement and dendritic spine immaturity. J. Neurosci. *27*, 9439–9450.

Kreis, T. E. (1987). Microtubules containing detyrosinated tubulin are less dynamic. EMBO J. *6*, 2597–2606.

Kuo, C. T., *et al.* (2006). Postnatal deletion of Numb/Numblike reveals repair and remodeling capacity in the subventricular neurogenic niche. Cell *127*, 1253–1264.

Lechtreck, K-F., Delmotte, P., Robinson, M. L., Sanderson, M. J., and Witman, G. B. (2008). Mutations in *Hydin* impair ciliary motility in mice. J. Cell Biol. *180*, 633–643.

Liu, A. X., Rane, N., Liu, J. P., and Prendergast, G. C. (2001). RhoB is dispensable for mouse development, but it modifies susceptibility to tumor formation as well as cell adhesion and growth factor signaling in transformed cells. Mol. Cell. Biol. *21*, 6906–6912.

Ma, X., Bao, J., and Adelstein, R. S. (2007). Loss of cell adhesion causes hydrocephalus in nonmuscle myosin II-B-ablated and mutated mice. Mol. Biol. Cell *18*, 2305–2312.

Marshall, W. F., and Nonaka, S. (2006). Cilia: tuning in to the cell's antenna. Curr. Biol. *16*, R604–R614.

Matter, K., and Balda, M. S. (2007). Epithelial tight junctions, gene expression and nucleo-junctional interplay. J. Cell Sci. *120*, 1505–1511.

Matter, K., Aijaz, S., Tsapara, A., and Balda, M. S. (2005). Mammalian tight junctions in the regulation of epithelial differentiation and proliferation. Curr. Opin. Cell Biol. *17*, 453–458.

Matter, K., McDowell, W., Schwarz, R. T., and Hauri. H.-P. (1989). Asynchronous transport to the cell surface of intestinal brush border hydrolases is not due to differential trimming of N-linked oligosaccharides. J. Biol. Chem. *264*, 13131–13139.

Nagatoya, K., Moriyama, T., Kawada, N., Takeji, M., Oseto, S., Murozono, T., Ando, A., Imai, E., and Hori, M. (2002). Y-27632 prevents tubulointerstitial fibrosis in mouse kidneys with unilateral ureteral obstruction. Kidney Int. *61*, 1684–1695.

Nechiporuk, T., Fernandez, T. E., and Vasioukhin, V. (2007). Failure of epithelial tube maintenance causes hydrocephalus and renal cysts in Dlg5−/− mice. Dev. Cell *13*, 338–350.

Nie, M., Aijaz, S., Leefa Chong San, I. V., Balda, M. S., and Matter, K. (2009) The Y-box factor ZONAB/DbpA associates with GEF-H1/Lfc and mediates Rho-stimulated transcription. EMBO Reports *10*, 1125–1131.

Odronitz, F., and Kollmar, M. (2007). Drawing the tree of eukaryotic life based on the analysis of 2,269 manually annotated myosins from 328 species. Genome Biol. *8*, R196.

Otani, T., Ichii, T., Aono, S., and Takeichi, M. (2006). Cdc42 GEF Tuba regulates the junctional configuration of simple epithelial cells. J. Cell Biol. *175*, 135–146.

Ozdamar, B., Bose, R., Barrios-Rodiles, M., Wang, H. R., Zhang, Y., and Wrana, J. L. (2005). Regulation of the polarity protein Par6 by TGFbeta receptors controls epithelial cell plasticity. Science *307*, 1603–1609.

Pinto, M., *et al.* (1983). Enterocyte-like differentiation and polarization of the human colon carcinoma cell-line CaCo-2 in culture. Biol. Cell *47*, 323–330.

Reinhard, J., Scheel, A. A., Diekmann, D., Hall, A., Ruppert, C., and Bähler, M. (1995). A novel type of myosin implicated in signaling by rho family GTPases. EMBO J. *14*, 697–704.

Rodríguez, C. I., Buchholz, F., Galloway, J., Sequerra, R., Kasper, J., Ayala, R., Stewart, A. F., and Dymecki, S. M. (2000). High-efficiency deleter mice show that FLPe is an alternative to Cre-loxP. Nat. Genet. *25*, 139–140.

Sahai, E., and Marshall, C. J. (2002). ROCK and Dia have opposing effects on adherens junctions downstream of Rho. Nat. Cell Biol. *4*, 408–415.

Samarin, S. N., Ivanov, A. I., Flatau, G., Parkos, C. A., and Nusrat, A. (2007). Rho/Rho-associated kinase-II signaling mediates disassembly of epithelial apical junctions. Mol. Biol. Cell *18*, 3429–3439.

Sapiro, R., Kostetskii, I., Olds-Clarke, P., Gerton, G. L., Radice, G. L., and Strauss, J. F., III. (2002). Male infertility, impaired sperm motility, and hydrocephalus in mice deficient in sperm-associated antigen 6. Mol. Cell. Biol. *22*, 6298–6305.

Schlessinger, K., Hall, A., and Tolwinski, N. (2009). Wnt signaling pathways meet Rho GTPases. Genes Dev. *23*, 265–277.

Shen, L., Black, E. D., Witkowski, E. D., Lencer, W. I., Guerriero, V., Schneeberger, E. E., and Turner, J. R. (2006). Myosin light chain phosphorylation regulates barrier function by remodeling tight junction structure. J. Cell Sci. *119*, 2095–2106.

Silva-Alvarez, C., *et al.* (2005). Ependymal cell differentiation and GLUT1 expression is a synchronous process in the ventricular wall. Neurochem. Res. *30*, 1227–1236.

Spassky, N., Merkle, F. T., Flames, N., Tramontin, A. D., Garcia-Verdugo, J. M., and Alvarez-Buylla, A. (2005). Adult ependymal cells are postmitotic and are derived from radial glial cells during embryogenesis. J. Neurosci. *25*, 10–18.

Suzuki, Y., Shibuya, M., Satoh, S., Sugiyama, H., Seto, M., and Takakura, K. (2008). Safety and efficacy of fasudil monotherapy and fasudil-ozagrel combination therapy in patients with subarachnoid hemorrhage: sub-analysis of the post-marketing surveillance study. Neurol. Med. Chir. *48*, 241–248.

Suzuki, Y., Shibuya, M., Satoh, S.-I., Sugimoto, Y., and Takakura, K. A. (2007). Postmarketing surveillance study of fasudil treatment after aneurismal subarachnoid hemorrhage. Surg. Neurol. *68*, 126–131.

Takaki, E., *et al.* (2007). Heat shock transcription factor 1 is required for maintenance of ciliary beating in mice. J. Biol. Chem. *282*, 37285–37292.

Town, T., *et al.* (2008). The stumpy gene is required for mammalian ciliogenesis. Proc. Natl. Acad. Sci. USA *105*, 2853–2858.

Tsapara, A., Matter, K., and Balda, M. S. (2006). The Heat Shock Protein Apg-2 Binds to the Tight Junction Protein ZO-1 and Regulates Transcriptional Activity of ZONAB. Mol. Biol. Cell *17*, 1322–1330.

Turner, J. R., Rill, B. K., Carlson, S. L., Carnes, D., Kerner, R., Mrsny, R. J., and Madara, J. L. (1997). Physiological regulation of epithelial tight junctions is associated with myosin light-chain phosphorylation. Am. J. Physiol. *273*, C1378–C1385.

Utech, M., Ivanov, A. I., Samarin, S. N., Bruewer, M., Turner, J. R., Mrsny, R. J., Parkos, C. A., and Nusrat, A. (2005). Mechanism of IFN-gamma-induced endocytosis of tight junction proteins: myosin II-dependent vacuolarization of the apical plasma membrane. Mol. Biol. Cell *16*, 5040–5052.

van de Wetering, M., *et al.* (1997). Armadillo coactivates transcription driven by the product of the *Drosophila* segment polarity gene dTCF. Cell *88*, 789–799.

Venugopalan, S. R., *et al.* (2008). Novel expression and transcriptional regulation of FoxJ1 during oro-facial morphogenesis. Hum. Mol. Genet. *17*, 3643–3654.

Woods, A., Sherwin, T., Sasse, R., MacRae, T. H., Baines, A. J., and Gull, K. (1989). Definition of individual components within the cytoskeleton of *Trypanosoma brucei* by a library of monoclonal antibodies. J. Cell Sci. *93*, 491–500.

Xing, H., Mayhew, C. N., Cullen, K. E., Park-Sarge, O. K., and Sarge, K. D. (2004). HSF-1 modulation of Hsp70 mRNA polyadenylation via interaction with symplekin. J. Biol. Chem. *279*, 10551–10555.

Yamada, S., and Nelson, W. J. (2007). Localized zones of Rho and Rac activities drive initiation and expansion of epithelial cell-cell adhesion. J. Cell Biol. *178*, 517–527.